PHILOSOPHICAL TRANSACTIONS B

royalsocietypublishing.org/journal/rstb

Research

Cite this article: El-Madany TS *et al*. 2020 Drought and heatwave impacts on semi-arid ecosystems' carbon fluxes along a precipitation gradient. *Phil. Trans. R. Soc. B* **375**: 20190519. http://dx.doi.org/10.1098/rstb.2019.0519

Accepted: 13 March 2020

One contribution of 16 to a theme issue 'Impacts of the 2018 severe drought and heatwave in Europe: from site to continental scale'.

Subject Areas:
environmental science

Keywords:
Iberian Peninsula, CO_2 flux, drought, heatwave, water stress, compound event

Author for correspondence:
Tarek S. El-Madany
e-mail: telmad@bgc-jena.mpg.de

Electronic supplementary material is available online at https://doi.org/10.6084/m9.figshare.c.5077598.

THE ROYAL SOCIETY PUBLISHING

Drought and heatwave impacts on semi-arid ecosystems' carbon fluxes along a precipitation gradient

Tarek S. El-Madany[1], Arnaud Carrara[2], M. Pilar Martín[3], Gerardo Moreno[4], Olaf Kolle[1], Javier Pacheco-Labrador[1], Ulrich Weber[1], Thomas Wutzler[1], Markus Reichstein[1] and Mirco Migliavacca[1]

[1]Department Biogeochemical Integration, Max Planck Institute for Biogeochemistry, Hans-Knöll Straße 10, 07745 Jena, Germany
[2]Centro de Estudios Ambientales del Mediterráneo (CEAM), Charles R. Darwin 14, 46980 Paterna, Valencia, Spain
[3]Environmental Remote Sensing and Spectroscopy Laboratory (SpecLab), Spanish National Research Council (CSIC), Albasanz 26-28, 28037 Madrid, Spain
[4]Forest Research Group, INDEHESA, University of Extremadura, Avda. Virgen del Puerto, 10600 Plasencia, Spain

TSE-M, 0000-0002-0726-7141; AC, 0000-0002-9095-8807; MPM, 0000-0002-5563-8461; GM, 0000-0001-8053-2696; OK, 0000-0002-7373-7519; JP-L, 0000-0003-3401-7081; TW, 0000-0003-4159-5445; MR, 0000-0001-5736-1112; MM, 0000-0003-3546-8407

The inter-annual variability (IAV) of the terrestrial carbon cycle is tightly linked to the variability of semi-arid ecosystems. Thus, it is of utmost importance to understand what the main meteorological drivers for the IAV of such ecosystems are, and how they respond to extreme events such as droughts and heatwaves. To shed light onto these questions, we analyse the IAV of carbon fluxes, its relation with meteorological variables, and the impact of compound drought and heatwave on the carbon cycle of two similar ecosystems, along a precipitation gradient. A four-year long dataset from 2016 to 2019 was used for the FLUXNET sites ES-LMa and ES-Abr, located in central (39°56′25″ N 5°46′28″ W) and southeastern (38°42′6″ N 6°47′9″ W) Spain. We analyse the physiological impact of compound drought and heatwave on the dominant tree species, *Quercus ilex*. Our results show that the gross primary productivity of the wetter ecosystem was less sensitive to changes in soil water content, compared to the dryer site. Still, the wetter ecosystem was a source of CO_2 each year, owing to large ecosystem respiration during summer; while the dry site turned into a CO_2 sink during wet years. Overall, the impact of the summertime compound event on annual CO_2 fluxes was marginal at both sites, compared to drought events during spring or autumn. This highlights that drought timing is crucial to determine the annual carbon fluxes in these semi-arid ecosystems.

This article is part of the theme issue 'Impacts of the 2018 severe drought and heatwave in Europe: from site to continental scale'.

1. Introduction

Semi-arid ecosystems play a major role for the inter-annual variability (IAV) of the terrestrial carbon sink [1,2]. Their IAV is driven by variations in precipitation and temperature. Owing to high rain-use efficiency [3], productivity can rapidly increase under conditions of high water availability, but just as quickly, the previously sequestered carbon can be released in drought years [4]. The importance of these compensatory effects on annual and seasonal fluxes, as well as the IAV is not yet understood and can be different depending on aridity regimes of the semi-arid ecosystems. Understanding the relevance of the timing of rainfall and extreme events (drought and/or heatwaves) during the year is indispensable. To determine the amount of annual precipitation at which an ecosystem changes from a carbon sink to a carbon source, Scott *et al*. [5] used linear regression between annual precipitation and net ecosystem productivity (NEP)

and showed that the carbon balance pivot point is variable. However, not only the annual precipitation determines their IAV of net ecosystem exchange of CO_2 (NEE), also the timing of precipitation and drought stress are important and influence ecosystem productivity and respiration in various ways. Firstly, the growing season length might be shortened when precipitation is scarce; secondly, the re-greening after the summer period might be delayed depending on timing and quantity of precipitation [6]; and thirdly, precipitation events during the dry season, so-called rain pulses, can result in large effluxes of CO_2 from soil. Additionally, further meteorological variables such as temperature and lag effects from previous seasons impact the seasonal ecosystem productivity [7]. By definition, semi-arid regions face drought stress during parts of the year and are thus prone to compound events of drought and heat stress [8], which reduce NEP [9]. Here, we analyse the different responses of CO_2 fluxes in two similar savannah type ecosystems in the central Iberian Peninsula, along a natural precipitation gradient, to (i) evaluate the impact and timing of drought on the IAV of NEE; (ii) identify the drivers of IAV of CO_2 fluxes; and (iii) compare the ecosystems' carbon and water flux responses during the compound event of heat- and drought stress in summer 2018, which was mainly driven by *Quercus ilex* trees.

2. Methods

(a) Site description

The two analysed ecosystems are located in western Spain and have the FLUXNET site identities ES-LMa and ES-Abr. ES-LMa is located close to the village of Majadas de Tiétar (39°56′25″ N 5°46′28″ W) and ES-Abr is located close to the village of La Albuera (38°42′6″ N 6°47′9″ W). Both ecosystems are savannah-like ecosystems, typical Iberian *dehesa*, which are tree-grass ecosystems used either for livestock grazing or agriculture. The two sites are located along a precipitation gradient with ES-LMa and ES-Abr getting an average precipitation of 650 and 350 mm yr^{-1} (with large IAV), respectively. The dominant tree species (greater than 98%) in both ecosystems are evergreen holm oaks (*Q. ilex*) with a height of 8.7 ± 1.3 m (ES-LMa) and 6.6 ± 0.9 m (ES-Abr) and a herbaceous layer [6,10]. The fractional canopy covers, based on terrestrial LiDAR scans, are 19.7 ± 4.9% and 24.4 ± 3.6% for ES-LMa and ES-Abr, respectively.

Soil at ES-LMa is classified as Abruptic Luvisol (WRB 2015), developed on Pliocene-Miocene alluvial deposits. The texture in the upper horizons is sandy (0–20 cm: 75% sand, 20% silt, 5% clay) and clayey (greater than 15% clay) from 30 to greater than 100 cm depth. The pH (measured in water extract) is approximately 5.5 in the first 20 cm, increasing to neutrality beneath 1 m depth. In ES-Abr, soil is classified as Chromic Acrisol, developed on Pliocene colluvial deposit, formed by a matrix of red clays with abundant stones of quartzite. While upper soils have similar texture between the sites, deeper soils differ. ES-LMa has a clay-rich deeper soil while ES-Abr contains gravel and stones, which facilitate rainwater infiltration to deeper layers.

The sites are influenced by the same large-scale synoptic conditions and have similar seasonal and phenological cycles, which are driven by the availability of water and timing of precipitation (electronic supplementary material, figure S1) with the difference that the herbaceous layer at ES-Abr usually senesces earlier [6]. During the summertime, temperature and solar radiation are high, while precipitation events are scarce. In this period, the herbaceous layer is senescent as the soil water content (SWC) is strongly reduced; whereas the evergreen *Q. ilex* trees survive through their ability to access deeper soil water reservoirs with their roots. When autumn rainfall begins and the soil is rewetted the herbaceous layer starts to green-up and biomass starts to buildup again [6]. The winter season is temperature and radiation limited with the majority of the annual precipitation falling during this period [7]. In spring, highest ecosystem productivity is observed owing to favourable water availability, as well as good temperature and radiation conditions for plant growth. The end of the growing period is then coupled to the reduction of available water, and increasing atmospheric water demand (vapour pressure deficit, VPD), which leads eventually to the senescence of the herbaceous layer.

(b) Heatwave 2018

The heatwave that struck the Iberian Peninsula in summer 2018 was relatively short with a duration of six days between 2 and 7 August. Nevertheless, the outstanding temperature amplitude resulted in many new absolute temperature records in western Iberia [11]. At both measurement sites, the heatwave was characterized by maximum air temperatures (T_a) above 40°C and maximum VPD higher than 70 hPa. Sousa *et al.* [11] describe the meteorological situation during the heatwave as a combination of a cyclonic circulation off the north-eastern Atlantic in combination with a strong subtropical ridge pattern over the affected area that promoted the advection of an anomalously warm air mass. For further details on the role of the intrusion of very warm and dry Saharan air masses in western Iberia and the extent of the 2018 heatwave see [11].

(c) Instrumentation and data processing

Instrumentation and data processing were identical at both measuring sites. Eddy covariance (EC) measurements were conducted with a sonic anemometer (R3–50 Gill Instruments, Lymingon UK) and an infra-red gas analyser (LI-7200, Licor Biosciences, Lincoln, USA) to calculate mass and energy fluxes of CO_2, latent heat (LE) and sensible heat (*H*). The measurement height was 15.5 and 12 m at ES-LMa and ES-Abr, respectively, corresponding to about 1.8 times the canopy height. At ES-LMa, an additional smaller EC system was installed at 1.6 m above ground in an open space sampling only the herbaceous layer. Flux calculations were performed with EddyPro v. 6.2.0 [12]. Raw time series were de-spiked, and block averaged means were subtracted, coordinate rotation was performed with the planar fit method [13] for the two main wind directions and the remaining data were rotated based on the double rotation method. Subsequently, data which were not fulfilling the assumptions of the EC methods [14] and data with low turbulent conditions [15] were removed from the dataset. Fluxes of CO_2 were storage corrected based on the single point storage correction in ES-Abr and with seven-point profile measurements in ES-LMa to derive NEE. The friction velocity (u^*)-threshold as well as its 5th and 95th percentiles were determined following Papale *et al.* [15]. Data below the respective u^*-thresholds were removed. The remaining data were gap-filled [16] and NEE was partitioned into gross primary productivity (GPP) and ecosystem respiration (Reco) based on the night time flux partitioning algorithm [16], using REddyProc v. 1.0.0 [17].

Uncertainties of cumulated NEE were estimated based on the spread of the 5th and 95th percentiles of the u^*-thresholds plus/minus the error propagation of the NEE uncertainty estimate from the marginal distribution sampling of the gap-filling algorithm [17]. As shown by El-Madany *et al.* [10] this uncertainty includes spatial, temporal and random uncertainties of the fluxes. For GPP and Reco, the spread of the uncertainty from the u^*-threshold estimation was used as for NEE. The same strategy was followed for calculating seasonal sums of carbon fluxes and the differences during drought and heatwave periods. Uncertainties were propagated following standard error propagation.

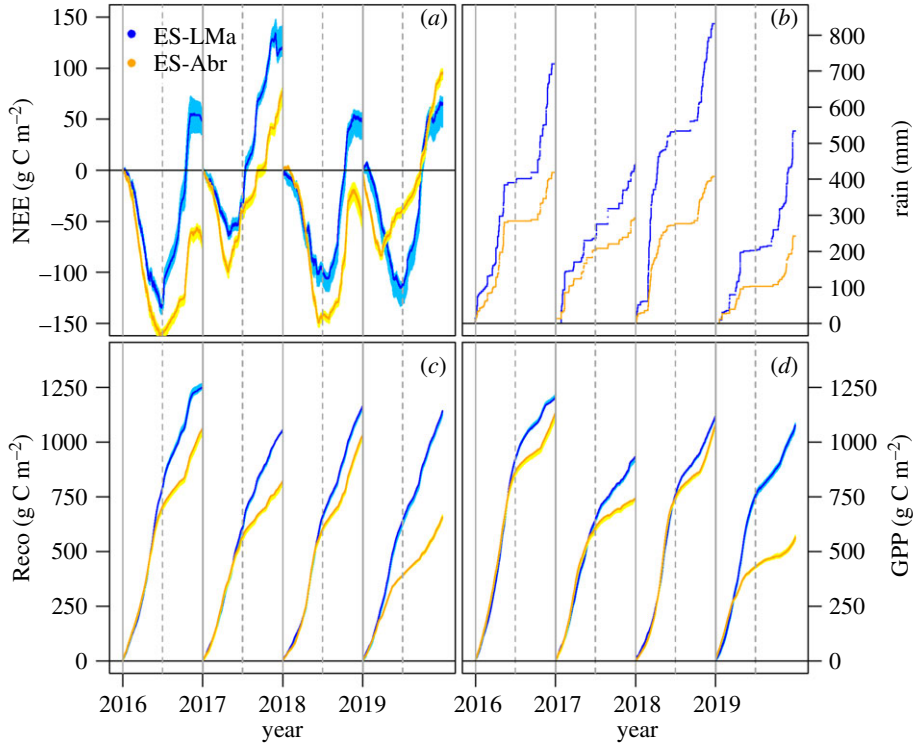

Figure 1. Cumulated fluxes of net ecosystem exchange (NEE; *a*), precipitation (rain; *b*), ecosystem respiration (Reco; *c*), and gross primary productivity (GPP; *d*) for ES-LMa in blue and ES-Abr in orange. Shaded areas represent propagated uncertainties based on u^*-threshold estimates and (for NEE) with random uncertainty of the flux measurements. (Online version in colour.)

Biometeorological measurements included air temperature (T_a) and relative humidity (rH) acquired at 2 m above ground, SWC at four locations and three depths at each location (5, 10 and 20 cm below ground), precipitation (*P*), pressure (Pa), and the short- and longwave incoming and outgoing radiation (SW_{in}, LW_{in}, SW_{up} and LW_{up}) components (CNR4, Kipp & Zonen, Delft, Netherlands). VPD was calculated from T_a and rH. All biometeorological data were collected at 10 s intervals and saved as 10 min averages, and then aggregated to 30 min averages to match the temporal resolution of the EC data.

SWC data were normalized to range from 0 to 1 where 1 corresponds to the 95th percentile of all data and thus to about the field capacity, while 0 corresponds to the 5th percentile of all data and consequently to completely dried soil. This method is possible owing to the large variability in SWC between the winter period, when soil is at field capacity, and the summer period when soil is reaching stable fully depleted SWC values. This was done for each measurement level (5, 10 and 20 cm) and then the normalized SWC (SWCn) values were averaged to represent the SWC of the rooting zone of the herbaceous layer (greater than 80% of the root length density accumulates within the top 20 cm of the soil [18]).

Sap flow measurements were performed with sap flow meters (SFM1, ITC International Pty Ltd, Armidale, Australia) based on the heat pulse method in six trees at each site [19]. Sap flow velocities were averaged for the inner and the outer measurement location within the sapwood. For each tree, mean diurnal cycles of sap velocities were calculated for the week of the heatwave and the week before and after the heatwave. The response of the trees to the heatwave was estimated based on the changes in sap velocity between the heatwave and the pre-heatwave period.

(d) Drivers of carbon fluxes

To identify the drivers of carbon fluxes a relative importance analysis (RIA) [20,21] was used on a basis of mean daily values. For each measurement site (ES-LMa, ES-Abr) mean daily values were calculated for NEE, GPP, Reco, SW_{in}, LW_{up}, net radiation (R_{net}), T_a, VPD, SWCn, soil heat flux (*G*) and wind speed. The relative importance (RI) of all variables as predictors for NEE, GPP and Reco was calculated using the *relaimpo* R-package [20]. The Lindeman, Merenda and Gold method (lmg) was used to calculate the contributions of each individual predictor variable to the total coefficient of determination (R^2). First, all contributions of the variables were averaged based on different orders of the predictor variables within one model. In a second step, the results of step one were averaged for each variable across multiple linear models of different sizes to account for potential correlation between the predictor variables. This procedure was done for each site individually and for each season as well as for the whole analysed period. This allows estimating (i) if certain variables are important throughout the year or only in certain seasons, (ii) if the two sites have the same main drivers, and (iii) how much of the carbon flux anomalies can be explained by the selected drivers.

3. Results

(a) Inter-annual variability of ecosystem carbon exchange

Annual NEE varied in the analysed period by 72 ± 8.6 and 154 ± 6.3 g C m^{-2} yr^{-1} in ES-LMa and ES-Abr, respectively (figure 1). While ES-LMa was every year a source of CO_2, ES-Abr was a carbon sink in wet years and a source in dry years. In dryer years, GPP at ES-LMa was more reduced than Reco which led to higher loss of carbon and thus more positive NEE (figure 1). The critical periods in which differences in NEE were built up between the two sites were winter and spring for the carbon uptake and summer for carbon losses (figures 1 and 2). Overall, both GPP and Reco were larger in ES-LMa when compared with ES-Abr.

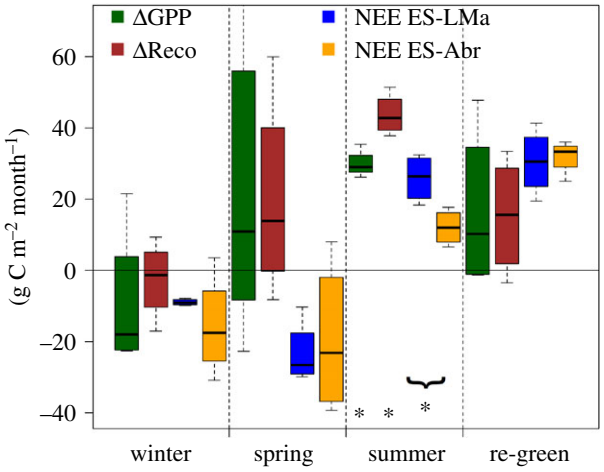

Figure 2. Boxplots of differences of gross primary productivity (ΔGPP; dark green) and ecosystem respiration (ΔReco; brown) between ES-LMa and ES-Abr, as well as net ecosystem exchange (NEE) for ES-LMa (blue) and ES-Abr (orange) for the periods winter (Dec, Jan, Feb), spring (Mar, Apr, May) summer (Jun, Jul, Aug, Sep) and re-greening (Oct, Nov). Each boxplot contains $n = 4$ data points, one for each year of the analysis. Seasonal values were calculated based on cumulated fluxes across the respective season. Differences (Δ) were calculated as ES-LMa − ES-Abr. Statistical test for mean values for ΔGPP and ΔReco being different from 0 were performed using a one-sample *t*-test and differences between NEE values were compared using a two-sample *t*-test. Asterisks below the boxplot show significance at the $p < 0.05$ level. (Online version in colour.)

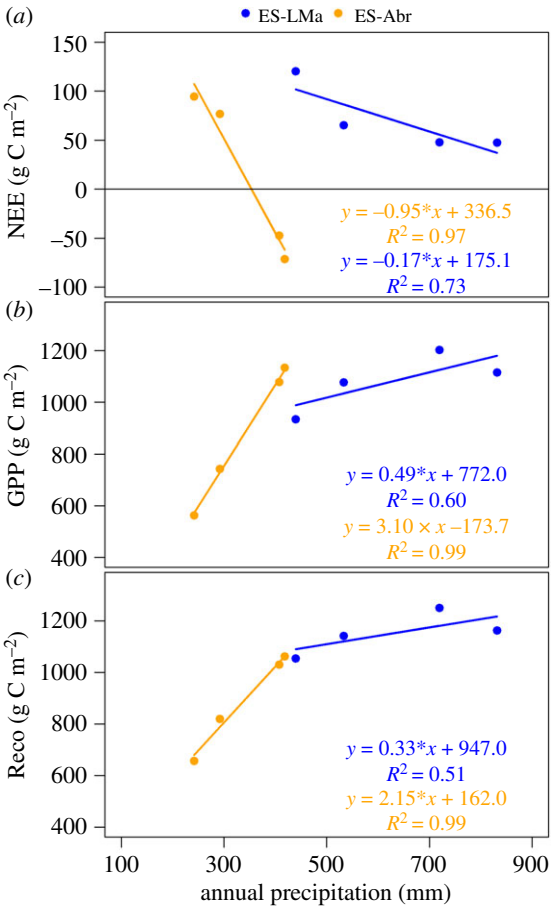

Figure 3. Correlation between annual net ecosystem exchange (NEE, *a*), gross primary productivity (GPP, *b*) and ecosystem respiration (Reco, *c*) and the annual precipitation for ES-LMa (blue) and ES-Abr (orange). Lines represent the linear regressions for each site in the respective colour code. (Online version in colour.)

The annual NEE at both sites is tightly coupled to the water availability (figure 1), as demonstrated by the strong linear relation between the annual precipitation and annual GPP and Reco (figure 3). At ES-Abr, R^2 between annual precipitation and GPP and Reco are 0.99 and 0.99, respectively, while they are 0.60 and 0.51 at ES-LMa (figure 3).

The wintertime was the only period during which median GPP was higher at ES-Abr when compared with ES-LMa (figure 2). Higher temperatures and SW_{in} at ES-Abr (electronic supplementary material, figure S1) were more favourable to build up biomass and fix carbon, especially by the herbaceous layer. This was emphasized by the high RI of SW_{in} and R_{net} for wintertime GPP at ES-Abr and ES-LMa (electronic supplementary material, figure S3). As a result, median NEE was more negative at ES-Abr than in ES-LMa indicating that during wintertime the dry site (ES-Abr) was a stronger sink than the wet site (ES-LMa).

During spring, GPP and Reco were larger in ES-LMa but median NEE was similar between the sites (figure 2 and table 1). The RIA shows that SWCn was the most important driver to explain variability in spring NEE, GPP and Reco at ES-Abr, while it was one of the least important ones at ES-LMa (electronic supplementary material, figure S3). The strong dependency of SWCn at ES-Abr then also translates into the spread of springtime NEE, i.e. the IAV which was twice as large as for ES-LMa (figure 2).

The summer period showed lowest IAV in NEE and most consistent differences between ES-LMa and ES-Abr (figure 2). The higher GPP at ES-LMa during the summer resulted from *Q. ilex* trees which were sequestering more carbon. The Reco exceeded GPP at both sites and resulted in positive NEE, but the median summer NEE was more than twice as large in ES-LMa (table 1). This systematic high Reco at ES-LMa during the long summers was not balanced by uptake during the growing periods, and thus the site behaved every year as a source of CO_2 (figure 1). Based on the RIA, the main driver for summertime Reco was, at both sites, SWCn. While for summertime GPP, SWCn was the most important variable at ES-Abr, it was the least important at ES-LMa.

During the re-greening, GPP and Reco were higher at ES-LMa but NEE was similar between the sites with large, but similar, IAV (figure 2). The median NEE at ES-LMa was similar to the summer period, while it was more than doubled at ES-Abr (table 1).

While SWCn is a relatively unimportant driver for carbon fluxes (at ES-LMa) during individual seasons, it is important at an annual timescale. Here, NEE, GPP and Reco are clearly driven by annual precipitation/SWCn (electronic supplementary material, figure S1 and figure 3) as shown by the high R^2 values (0.97, 0.99, 0.99 for NEE, GPP, Reco at ES-Abr and 0.73, 0.60, 0.51 for NEE, GPP, Reco at ES-LMa).

(b) Drought response

The SWCn is used here as indicator of water availability and potential drought stress. Within the period of 2016–2019, we observed for both sites two springs with above (2016 and 2018) and below (2017 and 2019) average SWCn (figure 4). Additionally, the complete autumn of 2017 was below average SWCn because autumn rains were strongly delayed and the re-wetting of the soil only happened in December.

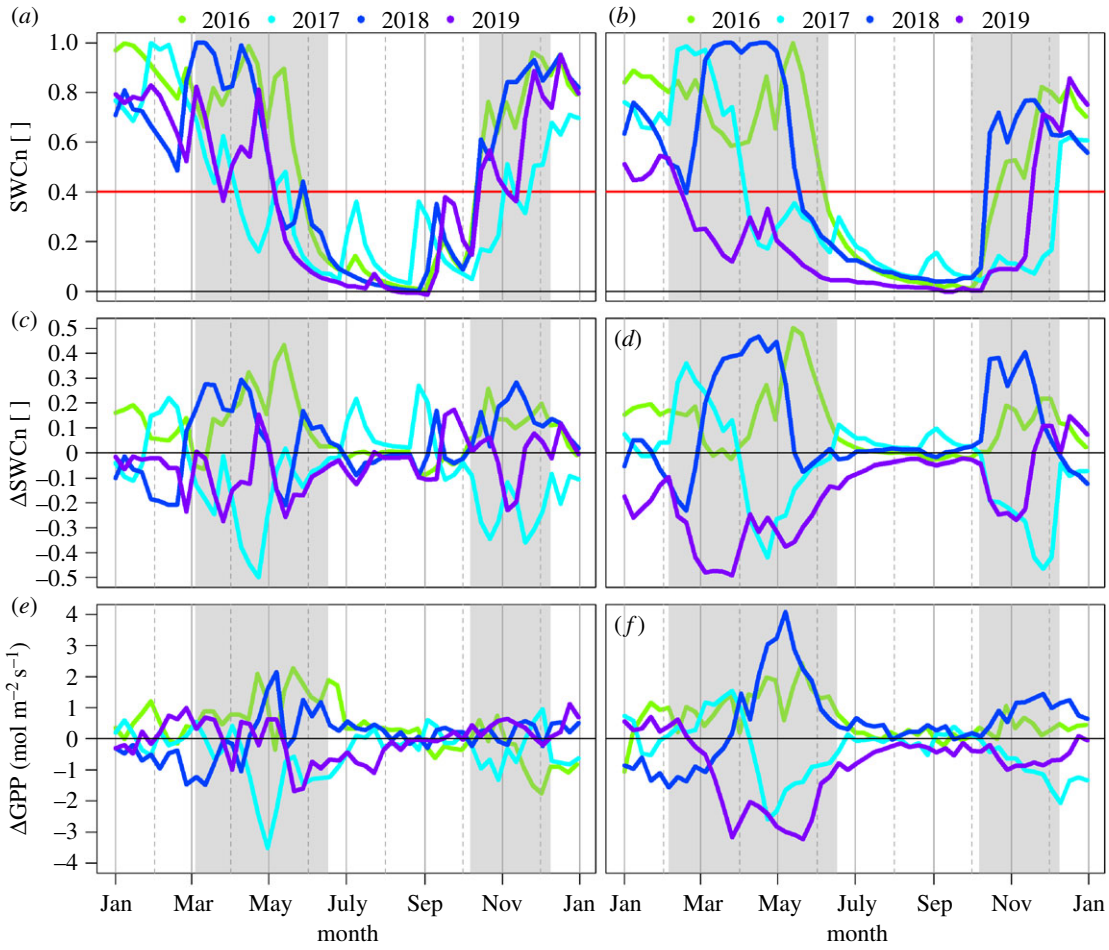

Figure 4. Normalized soil water content of the top 20 cm (SWCn, *a*,*b*). Anomalies of normalized soil water content (ΔSWCn, *c*,*d*) and gross primary productivity (ΔGPP, *e*,*f*) for ES-LMa (*a*,*c*,*e*) and ES-Abr (*b*,*d*,*f*). All time series are based on weekly averages. Each year is colour coded (light green 2016; light blue 2017, blue 2018, purple 2019). Grey shaded areas indicate the periods with high inter annual variability (corresponding to spring and autumn). Red horizontal line indicates the SWCn value, below which a reduction of GPP can be observed. (Online version in colour.)

Table 1. Impact of droughts during the autumn 2017 (Aut17), spring 2019 (Spr19) and the heatwave of summer 2018 (HW18, Sum18) on carbon fluxes (NEE, GPP, Reco) compared to the average of each season across all years (Aut, HW, Sum, Spr). (Values are cumulated for the period 1 October–30 November 2017 (Aut17), 2 August 2018 (HW18), 1 June–30 September 2018 (Sum18) and 1 March–31 May 2019 (Spr19) ± uncertainty. The same periods were selected for the seasonal averages but for all years. For a graphical representation of the values normalized to g C m^{-2} d^{-1} please see the electronic supplementary material, figure S7.)

	ΔNEE ES-Abr [g C m^{-2}]	ΔNEE ES-LMa [g C m^{-2}]	ΔGPP ES-Abr [g C m^{-2}]	ΔGPP ES-LMa [g C m^{-2}]	ΔReco ES-Abr [g C m^{-2}]	ΔReco ES-LMa [g C m^{-2}]
Aut17	−14.5 ± 3.4	−1.8 ± 6.2	−37.9 ± 4.7	−28.1 ± 1.3	−52.4 ± 10.1	−29.9 ± 8.4
HW18	+3.2 ± 0.4	+2.3 ± 0.8	−0.7 ± 0.6	+0.7 ± 1.1	+2.5 ± 0.7	+3.0 ± 1.2
Sum18	−9.8 ± 4.3	−32.3 ± 12.0	+49.0 ± 2.3	+43.1 ± 4.1	+39.2 ± 5.8	+10.8 ± 6.8
Spr19	+83.6 ± 6.7	−15.3 ± 10.9	−216.1 ± 12.3	−2.1 ± 5.6	−132.5 ± 10.7	−17.6 ± 7.6
Aut	+63.2 ± 3.0	+61.8 ± 5.6	73.3 ± 1.2	107.3 ± 0.5	136.5 ± 2.8	168.6 ± 0.9
HW	+3.0 ± 0.1	+4.7 ± 0.4	5.0 ± 0.1	8.7 ± 0.3	7.9 ± 0.1	13.4 ± 0.3
Sum	+48.1 ± 3.6	+103.9 ± 11.6	147.5 ± 1.0	267.9 ± 1.5	195.6 ± 1.8	371.8 ± 2.6
Spr	−57.8 ± 6.4	−70.5 ± 10.3	415.5 ± 3.6	488.0 ± 2.1	357.7 ± 2.9	417.5 ± 2.9

The periods with positive SWCn anomalies (ΔSWCn) resulted in positive anomalies in GPP (ΔGPP), and vice versa. This relation was more pronounced in ES-Abr than in ES-LMa as shown by the higher correlation coefficient ($R^2 = 0.44$, $R^2 = 0.05$, for ES-Abr, ES-LMa) and the steeper slope (3.84 ± 0.30, 1.28 ± 0.38, for ES-Abr, ES-LMa) of the linear regression between ΔSWCn and ΔGPP (electronic supplementary material, figure S2). The same is true for the relation between ΔSWCn and ΔReco at both sites ($R^2 = 0.51, 0.16$; slopes = 2.91 ± 0.19, 2.13 ± 0.34; electronic supplementary material, figure S2, for ES-Abr, ES-LMa, respectively). Based on an ANCOVA, the slopes between

ΔSWCn and ΔGPP are significantly different ($p < 0.001$) while they are not for ΔSWCn and ΔReco ($p > 0.1$). It should be noted, that for ES-Abr the slope between ΔSWCn and ΔReco is lower than that of ΔSWCn and ΔGPP, while it is the opposite for ES-LMa. Therefore, under positive ΔSWCn the increase of GPP exceeds that of Reco while in periods with negative SWCn anomalies it is the opposite, for ES-Abr. As a result, ES-Abr becomes a carbon sink in wet years (2016 and 2018) while it becomes a carbon source in dry years (2017 and 2019), as shown in figure 1. For ES-LMa, the increase of Reco under wet conditions is larger when compared with that of GPP (electronic supplementary material, figure S2). Which seems contradictory to the annual scale at which GPP is increasing more strongly with increasing annual precipitation when compared with Reco. The background Reco (offset in the linear regression equation) at ES-LMa (figure 3) is 175 g C m^{-2} higher than that of GPP and thus ES-LMa stays a carbon source in all analysed years. The higher slope of the short-term relation of ΔSWCn and ΔReco (electronic supplementary material, figure S2) translates into the large Reco offset at an annual scale (figure 3).

The carbon fluxes in ES-Abr were more strongly affected by drought conditions when compared with ES-LMa which is expected as the SWCn is the most important variable for changes in carbon fluxes (electronic supplementary material, figure S3). The strongest reduction in carbon fluxes was observed at ES-Abr during the 2019 spring drought when GPP was reduced by 216.1 ± 12.3 g C m^{-2} and Reco by 132.5 ± 10.7 g C m^{-2}, which corresponds to 52% of average springtime GPP and 37% of Reco (table 1). Overall, this stronger impact on GPP when compared with Reco turned NEE during this period from an average carbon sink (−57.8 ± 6.4 g C m^{-2}) to a source (25.8 ± 6.7 g C m^{-2}). Even though precipitation was also scarce at ES-LMa during this period, Reco was more strongly reduced than GPP which resulted even in slightly more carbon uptake (ΔNEE = −15.3 ± 10.9 g C m^{-2}).

During the dry autumn of 2017 GPP and Reco were reduced at both sites. At ES-LMa, their reduction was similar (ΔGPP = −28.1 ± 1.3 g C m^{-2} (26%), ΔReco = −29.9 ± 8.4 g C m^{-2} (18%)) and thus ΔNEE barely changed (−1.8 ± 6.2 g C m^{-2}). At ES-Abr, the response was stronger in relative and absolute terms with −37.9 ± 4.7 g C m^{-2} (51%, GPP) and −52.4 ± 10.1 g C m^{-2} (38%, Reco), leading to a negative ΔNEE (−14.5 ± 3.4 g C m^{-2}) but still positive absolute NEE during autumn 2019.

During summer 2018, both sites increased GPP and Reco compared to the average, but with a stronger increase in GPP when compared with Reco (table 1). Overall, ΔNEE was −9.8 ± 4.3 and −32.3 ± 12.0 g C m^{-2} during summer 2018 at ES-Abr and ES-LMa, respectively. This is contradictory to the period of the heatwave during which the increase of Reco dominated the ecosystem response at both sites (+2.5 ± 0.7 and +3.0 ± 1.2 g C m^{-2} in 6 days at ES-Abr and ES-LMa). But the short period and its potential lag effects did not impact the overall carbon fluxes during the summer 2018.

(c) Effects of compound drought and heatwave event 2018

The 2018 heatwave was a compound event as it struck the Iberian Peninsula during the summer drought period. The compound event only marginally affected the summer 2018 NEE at the sites and even less the annual NEE owing to its short duration. The ecosystem response to that event can be attributed to soil processes and the physiological response of the tree layer because the herbaceous layer was already senesced. During the heatwave, T_a and VPD increased strongly compared to the pre-heatwave period. Increases were higher at ES-Abr, than at ES-LMa (figure 5; electronic supplementary material, figure S4). T_a and VPD during the heatwave were 4.3°C and 11.5 hPa higher at ES-LMa and 7.1°C and 19 hPa higher at ES-Abr.

During the pre-heatwave period, mean daytime GPP was, on average, 1.38 µmol m^{-2} s^{-1} larger at ES-LMa than at ES-Abr (figure 5). However, the patterns of the fluxes were similar between sites. Highest GPP values occur at both sites already between 9.00 and 10.00 Universal Time, coordinated (UTC) and reduced afterwards with increasing T_a, SW_{in} and VPD. During the heatwave, diurnal patterns of the fluxes were different between the sites (figure 5). While the diurnal pattern of GPP stayed the same at ES-LMa and only the magnitude was reduced by about 1 µmol m^{-2} s^{-1}, a strong change in the pattern and magnitude of about 1–3 µmol m^{-2} s^{-1} was observed at ES-Abr. Here, the peak of GPP only reached up to 2.5 µmol m^{-2} s^{-1} and then dropped rapidly to about 1 µmol m^{-2} s^{-1} and remained constant until sunset (figure 5). This response of the trees at ecosystem scale was in line with independent sap flow measurements at the two sites, which showed stronger reduced sap flows at ES-Abr during day- and even during night-time hours. The *Q. ilex* trees at both sites increased their sap flow directly after sunrise for about two hours which corresponded to the period with highest GPP during the heatwave period. Overall, mean GPP was reduced during the heatwave by 0.81 µmol m^{-2} s^{-1} and 0.49 µmol m^{-2} s^{-1} which corresponded to over 40% and about 15% at ES-Abr and ES-LMa, respectively.

After the compound event, the ecosystems did not rebound to pre-heatwave conditions (electronic supplementary material, figure S5), even though GPP increased compared to the heatwave, because drought stress was still present and caused a further reduction of GPP until precipitation fell in September and relieved the drought stress.

4. Discussion

(a) Inter annual variability

Increasing drought conditions over the Iberian Peninsula [8,22] will eventually result in less water availability and thus impact the carbon sequestration potential. It was shown for various semi-arid ecosystems that in dry years, delayed timing of precipitation or lower annual precipitation reduce the growing season length and thus GPP and NEP [5,23,24]. Depending on drought length and intensity this can even change the ecosystems from being a carbon sink to a carbon source [5] as is the case for ES-Abr (figures 1 and 3). While the inflection point between a sink and a source is for ES-Abr around 350 mm of annual precipitation, it was not reached for ES-LMa at 830 mm. Comparing this value to other tree grass ecosystems around the globe, the value is rather high [5,23,25,26]. The positive NEE values, responsible for the high Reco (figures 1 and 2), especially during summer, are not driven by subterranean ventilation [27,28] as the soil characteristics are not favourable for

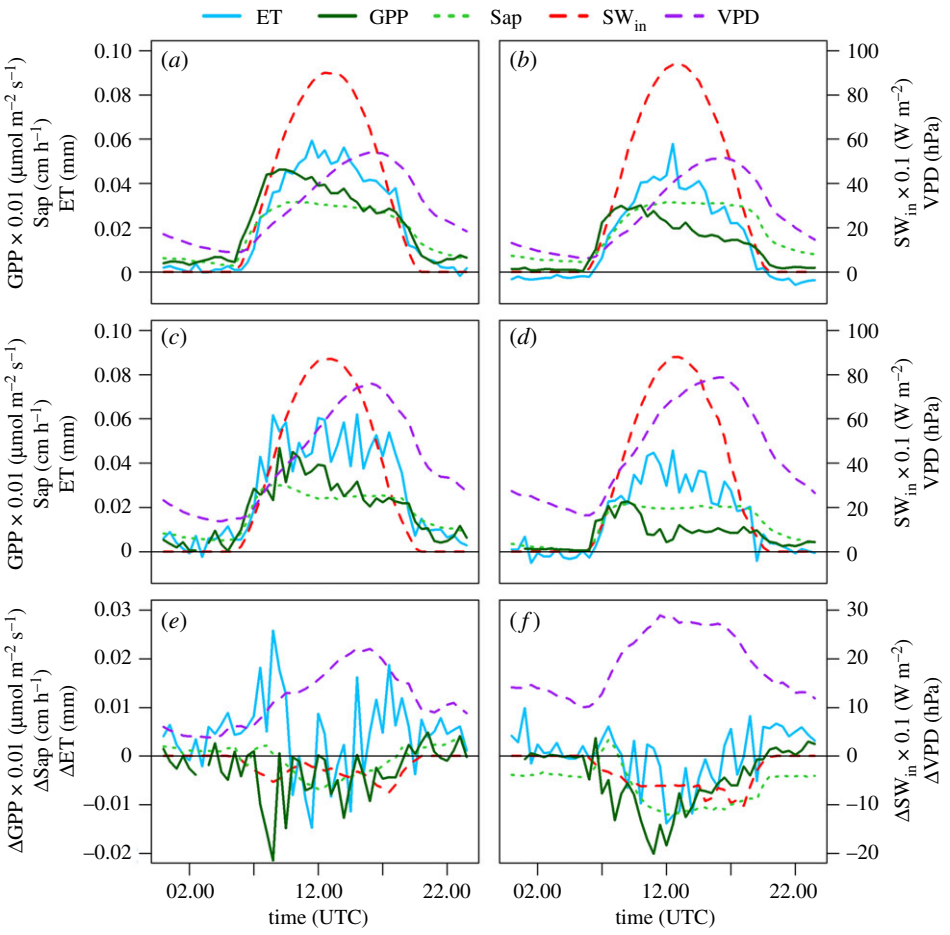

Figure 5. Mean diel cycles of evapotranspiration (ET; light blue), gross primary productivity (GPP; dark green), sap velocity (Sap; light green dotted), short wave incoming radiation (SW_{in}; red dashed), and vapour pressure deficit (VPD; purple dashed), for the period before the heatwave (*a*,*b*), the heatwave (*c*,*d*), and the changes in these variables from before the heatwave to during the heatwave period (i.e. heatwave—pre-heatwave) for ES-LMa (*a*,*c*,*e*) and ES-Abr (*b*,*d*,*f*). (Online version in colour.)

this process and the relation between NEE and wind speed is not as expected for this process (electronic supplementary material, figure S6). Thus, we have to assume that high Reco is driven by biological processes. One reason for the higher Reco in ES-LMa during the summer could be a lagged effect from the higher productivity during the spring period. But, the ratio of summer NEE to spring NEE (table 1) shows that ES-LMa loses on average more carbon during summer as it is taking up during the spring, while it is the opposite for ES-Abr. This indicates that the higher Reco at ES-LMa is not driven by higher productivity during spring but by other processes which are not related to vegetation but rather to the soil.

The overall variability of GPP during summer is low compared to other seasons (figure 4; electronic supplementary material, figure S1) and thus not adding much signal to the IAV of the sites. This is especially true when comparing these semi-arid ecosystems, which are adapted to summertime drought and heat stress, with other ecosystems which are usually active during summer and are stressed by e.g. a drought or heat as in summer 2018 [29–31]. In fact, the summer of 2018 was more productive than the average at the sites (table 1) and for the whole Iberian Peninsula [29].

The strong dependency of carbon fluxes at ES-Abr to SWCn (figure 4; electronic supplementary material, figures S2 and S3) translates into larger variability of NEE, GPP and Reco at an annual timescale (figures 1 and 3). The range between the smallest and the largest annual sums are more than the double at ES-Abr compared to ES-LMa. This supports the concepts of reduced rain-use-efficiency with increasing precipitation and the positive asymmetry in ecosystem response to rainfall [3,32]. In accordance with the former, the relation of GPP and Reco with annual precipitation (figure 3) cannot be expected to follow a linear relation. A convergence to an upper limit of productivity can be assumed even if precipitation increases further. On the other hand, GPP and Reco will not follow the linear relation but will converge faster towards 0 if no water is available for longer periods. For shorter periods, legacy effects must be considered [7,33,34] as they will impact these relations. A longer dataset of these similar sites with more positive and negative precipitation extremes will surely help to better understand the processes and impacts of precipitation to the carbon cycle.

(b) Ecosystem response to drought and heatwave

The relevance that heat and drought events have on ecosystem functioning as well as their imprint on the carbon cycle was well described in a recent review [35]. However, only little is known about the different responses to drought along a precipitation gradient for elsewise similar ecosystems. The two analysed drought cases of spring 2019 and autumn 2017 show how important timing and amount of precipitation is during these seasons for driving phenology, ecosystem carbon fluxes and eventually the annual carbon

sequestration. The herbaceous layers at both sites cannot access deep soil water owing to their root density profiles [18,36]. However, at ES-LMa precipitation falls more frequently and at higher quantity (figure 1; electronic supplementary material, figure S1), therefore the herbaceous layer can develop better and average spring and autumn GPP are higher (table 1). As a result, ES-Abr is more sensitive to variability in SWCn in spring and autumn.

During summer, higher GPP at ES-LMa indicates that the *Q. ilex* trees were less stressed when compared with those at ES-Abr. Water availability from deeper soil layers at ES-LMa and potentially enhanced water saving strategies to drier conditions at ES-Abr are the most plausible explanations, as the canopy cover between the sites is similar and rather lower at ES-LMa. The low variability of ΔGPP and ΔReco (figure 2, summer) indicates that *Q. ilex* at ES-LMa and ES-Abr were responding similarly to summer drought and heat stress conditions during the four analysed years. This is emphasized by the decaying pattern of mean daily GPP during summer 2018 (electronic supplementary material, figure S5) under which also the higher GPP at ES-LMa is obvious. At the same time, this leads to the conclusion that the herbaceous layer is responsible for the large variability in ΔGPP and ΔReco during the other seasons (figure 2).

Felton & Smith [37] highlight the importance of integrating responses to climate extremes from plant to ecosystem scale and this is where the analysis of the 2018 heatwave contributes. During the summer the ecosystems are thought to be *dormant* and only *Q. ilex* trees which are well adapted to heat and drought are active but their response to the heatwave were different at the sites. The 2018 heatwave was exceptional. Even globally, there is little literature to compare our results to, as conditions of VDP values above 70 hPa and T_a above 40°C are rare. Regular VDP values range in drought and heat stress studies between 40 to 50, seldom up to 60 hPa [24,38–41]. As a response, the trees show an extreme stomatal regulation of the CO_2 uptake and water loss during the heatwave as shown for other xeric species [42,43]. The stronger physiological response at ES-Abr when compared with ES-LMa (greater reduction in sap flow and GPP) could be associated with the higher atmospheric demand at ES-Abr and to the availability of deeper soil water in ES-LMa. Furthermore, the differences in nocturnal sap flow patterns suggest stronger rehydration of the tree tissues in ES-LMa, while even this water transport was reduced at ES-Abr owing to strong water limitation. The only increase in sap flow during the heatwave was detected at both sites shortly after sunrise for about 2 h and corresponded to an increase in GPP (see above). This early morning sap flow increase was more pronounced at ES-Abr than at ES-LMa and was a result of a faster sap flow increase directly linked to sunrise and increasing SW_{in}. This response at ES-Abr might be an indication of the stress and physiological struggle between dehydration and starving.

5. Conclusion

The availability of water in semi-arid ecosystems and the timing of drought are of major importance for the carbon cycle and its IAV. Nevertheless, wetter ecosystems are not necessarily able to sequester more carbon. In ecosystems where GPP and Reco are tightly coupled, the inhibition of Reco in dryer ecosystems can, as shown in this study, have a major impact on the annual NEE and result in larger carbon sequestration. The summer period during which semi-arid ecosystems are thought to be dormant can be of high relevance for the carbon exchange owing to the dominance of Reco over GPP. Still, ES-Abr is more sensible to drought, especially during spring and autumn and thus IAV of NEE, GPP and Reco increases.

We show that in seasonally dry ecosystems, the timing of droughts is fundamental to determine the annual impact on the carbon fluxes. Therefore, for the carbon fluxes, in these ecosystems droughts in autumn and spring require more attention than summertime ones. The compound event of drought and heat during the summer of 2018 only marginally impacted the annual NEE. However, for this event, the evergreen trees at the site had a critical role in the modulation of the ecosystem response, especially at the dryer site where water stress was even stronger. At ecosystem scale, the wetter site lost more carbon, however, the trees benefit from the higher water availability during summer and even during compound drought and heat events.

Data accessibility. The used dataset is available at: https://zenodo.org/record/3707842#.XmqduEpCe70.

Authors' contributions. All authors helped with data analysis and with writing and improving a former version of this manuscript. M.R., M.M., A.C. and T.S.E.-M. conceived and designed the study. T.S.E.-M. wrote a former version of this manuscript and performed the analysis. A.C. collected and provided data for ES-LMa. O.K. and M.M. collected and provided data for ES-Abr. G.M. did soil sampling, soil analysis and classifications at both sites.

Competing interests. We declare we have no competing interests.

Funding. T.S.E.-M. and M.M. acknowledge financial support through Project no. 404943228 of the Deutsche Forschungsgemeinschaft. M.P.M. thanks MINECO/FEDER, UE funding support through SynerTGE project (CGL2015-69095-R). G.M. acknowledges financial support from the grant Agreement IB16185 of the Regional Government of Extremadura.

Acknowledgements. The authors thank Ramón López-Jimenez, Martin Hertel, Martin Strube, Oscar Perez-Priego, Yonatan Cáceres and Enrique Juarez for great support during fieldwork. T.S.E.-M. and M.M. thank Ekaterina Bogdanovich and Marcus Guderle for processing and analysing terrestrial LiDAR scans to derive fractional canopy cover for ES-LMa and ES-Abr. Additionally, T.S.E.-M., M.M. and M.R. thank the Alexander von Humbold Stiftung for financial support of the MaNiP project. A.C. thanks projects IMAGINA (PROMETEU 2019, Generalitat Valenciana) and ELEMENTAL (CGL 2017-83538-C3-3-R, MINECO-FEDER).

References

1. Ahlstrom A *et al.* 2015 The dominant role of semi-arid ecosystems in the trend and variability of the land CO_2 sink. *Science* **348**, 895–899. (doi:10.1126/science.aaa1668)
2. Poulter B *et al.* 2014 Contribution of semi-arid ecosystems to interannual variability of the global carbon cycle. *Nature* **509**, 600–603. (doi:10.1038/nature13376)
3. Huxman TE *et al.* 2004 Convergence across biomes to a common rain-use efficiency. *Nature* **429**, 651–654. (doi:10.1038/nature02561)

4. Ma X *et al.* 2016 Drought rapidly diminishes the large net CO_2 uptake in 2011 over semi-arid Australia. *Sci. Rep.* **6**, 37747. (doi:10.1038/srep37747)
5. Scott RL, Biederman JA, Hamerlynck EP, Barron-Gafford GA. 2015 The carbon balance pivot point of southwestern U.S. semiarid ecosystems: insights from the 21st century drought. *J. Geophys. Res. Biogeosci.* **120**, 2612–2624. (doi:10.1002/2015JG003181)
6. Luo Y *et al.* 2018 Using near-infrared-enabled digital repeat photography to track structural and physiological phenology in Mediterranean tree–grass ecosystems. *Remote Sensing* **10**, 1293. (doi:10.3390/rs10081293)
7. Sippel S *et al.* 2017 Warm winter, wet spring, and an extreme response in ecosystem functioning on the Iberian Peninsula. *Bull. Am. Meteorol. Soc.* **98**, chapter 16. (doi:10.1175/BAMS-D-17-0135.1)
8. Hao Z, Hao F, Singh VP, Zhang X. 2018 Changes in the severity of compound drought and hot extremes over global land areas. *Environ. Res. Lett.* **13**, 124022. (doi:10.1088/1748-9326/aaee96)
9. von Buttlar J *et al.* 2018 Impacts of droughts and extreme-temperature events on gross primary production and ecosystem respiration: a systematic assessment across ecosystems and climate zones. *Biogeosciences* **15**, 1293–1318. (doi:10.5194/bg-15-1293-2018)
10. El-Madany TS *et al.* 2018 Drivers of spatio-temporal variability of carbon dioxide and energy fluxes in a Mediterranean savanna ecosystem. *Agric. For. Meteorol.* **262**, 258–278. (doi:10.1016/j.agrformet.2018.07.010)
11. Sousa PM, Barriopedro D, Ramos AM, García-Herrera R, Espírito-Santo F, Trigo RM. 2019 Saharan air intrusions as a relevant mechanism for Iberian heatwaves: the record breaking events of August 2018 and June 2019. *Weather Clim. Extremes* 100224-100237. (doi:10.1016/j.wace.2019.100224)
12. Fratini G, Mauder M. 2014 Towards a consistent eddy-covariance processing: an intercomparison of EddyPro and TK3. *Atmos. Meas. Tech.* **7**, 2273–2281. (doi:10.5194/amt-7-2273-2014)
13. Wilczak JM, Oncley SP, Stage SA. 2001 Sonic anemometer tilt correction algorithms. *Boundary Layer Meteorol.* **99**, 127–150. (doi:10.1023/A:1018966204465)
14. Foken T, Göckede M, Mauder M, Mahrt L, Amiro BD, Munger JW. 2004 Post-field data quality control. In *Handbook of micrometeorology: a guide for surface flux measurement and analysis* (eds X Lee, W Massman, B Law), pp. 181–208. Dordrecht, the Netherlands: Kluwer Academic Publishers.
15. Papale D *et al.* 2006 Towards a standardized processing of net ecosystem exchange measured with eddy covariance technique: algorithms and uncertainty estimation. *Biogeosciences* **3**, 571–583. (doi:10.5194/bg-3-571-2006)
16. Reichstein M *et al.* 2005 On the separation of net ecosystem exchange into assimilation and ecosystem respiration: review and improved algorithm. *Glob. Change Biol.* **11**, 1424–1439. (doi:10.1111/j.1365-2486.2005.001002.x)
17. Wutzler T, Lucas-Moffat A, Migliavacca M, Knauer J, Sickel K, Šigut L, Menzer O, Reichstein M. 2018 Basic and extensible post-processing of eddy covariance flux data with REddyProc. *Biogeosciences* **15**, 5015–5030. (doi:10.5194/bg-15-5015-2018)
18. Rolo V, Moreno G. 2012 Interspecific competition induces asymmetrical rooting profile adjustments in shrub-encroached open oak woodlands. *Trees* **26**, 997–1006. (doi:10.1007/s00468-012-0677-8)
19. Perez-Priego O *et al.* 2017 Evaluation of eddy covariance latent heat fluxes with independent lysimeter and sapflow estimates in a Mediterranean savannah ecosystem. *Agric. For. Meteorol.* **236**, 87–99. (doi:10.1016/j.agrformet.2017.01.009)
20. Grömping U. 2006 Relative importance for linear regression in R: the package relaimpo. *J. Stat. Softw.* **17**, 1–27. (doi:10.18637/jss.v017.i01)
21. Grömping U. 2015 Variable importance in regression models. *Wiley Interdiscip. Rev. Comput. Stat.* **7**, 137–152. (doi:10.1002/wics.1346)
22. Coll JR, Aguilar E, Ashcroft L. 2017 Drought variability and change across the Iberian Peninsula. *Theor. Appl. Climatol.* **130**, 901–916. (doi:10.1007/s00704-016-1926-3)
23. Ma S, Baldocchi DD, Xu L, Hehn T. 2007 Inter-annual variability in carbon dioxide exchange of an oak/grass savanna and open grassland in California. *Agric. For. Meteorol.* **147**, 157–171. (doi:10.1016/j.agrformet.2007.07.008)
24. Cleverly J *et al.* 2016 Productivity and evapotranspiration of two contrasting semiarid ecosystems following the 2011 global carbon land sink anomaly. *Agric. For. Meteorol.* **220**, 151–159. (doi:10.1016/j.agrformet.2016.01.086)
25. Pereira JS *et al.* 2007 Net ecosystem carbon exchange in three contrasting Mediterranean ecosystems: the effect of drought. *Biogeosciences* **4**, 791–802. (doi:10.5194/bg-4-791-2007)
26. Luo H, Oechel WC, Hastings SJ, Zulueta R, Qian Y, Kwon H. 2007 Mature semiarid chaparral ecosystems can be a significant sink for atmospheric carbon dioxide. *Glob. Change Biol.* **13**, 386–396. (doi:10.1111/j.1365-2486.2006.01299.x)
27. Serrano-Ortiz P, Domingo F, Cazorla A, Were A, Cuezva S, Villagarcía L, Alados-Arboledas L, Kowalski AS. 2009 Interannual CO_2 exchange of a sparse Mediterranean shrubland on a carbonaceous substrate. *J. Geophys. Res.* **114**, 1–11. (doi:10.1029/2009JG000983)
28. López-Ballesteros A, Serrano-Ortiz P, Kowalski AS, Sánchez-Cañete EP, Scott RL, Domingo F. 2017 Subterranean ventilation of allochthonous CO_2 governs net CO_2 exchange in a semiarid Mediterranean grassland. *Agric. For. Meteorol.* **234–235**, 115–126. (doi:10.1016/j.agrformet.2016.12.021)
29. Bastos A *et al.* 2020 Impacts of extreme summers on European ecosystems: a comparative analysis of 2003, 2010 and 2018. *Phil. Trans. R. Soc. B* **375**, 20190507. (doi:10.1098/rstb.2019.0507)
30. Fu Z *et al.* 2020 Sensitivity of gross primary productivity to climatic drivers during the summer drought of 2018 in Europe. *Phil. Trans. R. Soc. B* **375**, 20190747. (doi:10.1098/rstb.2019.0747)
31. Beillouin D, Schauberger B, Bastos A, Ciais P, Makowski D. 2020 Impact of extreme weather conditions on European crop production in 2018. *Phil. Trans. R. Soc. B* **375**, 20190510. (doi:10.1098/stb.2019.0510)
32. Haverd V, Ahlström A, Smith B, Canadell JG. 2017 Carbon cycle responses of semi-arid ecosystems to positive asymmetry in rainfall. *Glob. Change Biol.* **23**, 793–800. (doi:10.1111/gcb.13412)
33. Delgado-Balbuena J, Arredondo JT, Loescher HW, Pineda-Martínez LF, Carbajal JN, Vargas R. 2019 Seasonal precipitation legacy effects determine the carbon balance of a semiarid grassland. *J. Geophys. Res. Biogeosci.* **124**, 987–1000. (doi:10.1029/2018JG004799)
34. Correia AC, Costa-e-Silva F, Dubbert M, Piayda A, Pereira JS. 2016 Severe dry winter affects plant phenology and carbon balance of a cork oak woodland understorey. *Acta Oecologica* **76**, 1–12. (doi:10.1016/j.actao.2016.07.004)
35. Sippel S, Reichstein M, Ma X, Mahecha MD, Lange H, Flach M, Frank D. 2018 Drought, heat, and the carbon cycle: a review. *Curr. Clim. Change Rep.* **4**, 266–286. (doi:10.1007/s40641-018-0103-4)
36. Nair RKF, Morris KA, Hertel M, Luo Y, Moreno G, Reichstein M, Schrumpf M, Migliavacca M. 2019 N: P stoichiometry and habitat effects on Mediterranean savanna seasonal root dynamics. *Biogeosciences* **16**, 1883–1901. (doi:10.5194/bg-16-1883-2019)
37. Felton AJ, Smith MD. 2017 Integrating plant ecological responses to climate extremes from individual to ecosystem levels. *Phil. Trans. R. Soc. B* **372**, 20160142. (doi:10.1098/rstb.2016.0142)
38. Zhang Q, Ficklin DL, Manzoni S, Wang L, Way D, Phillips RP, Novick KA. 2019 Response of ecosystem intrinsic water use efficiency and gross primary productivity to rising vapor pressure deficit. *Environ. Res. Lett.* **14**, 074023. (doi:10.1088/1748-9326/ab2603)
39. Sulman BN, Roman DT, Yi K, Wang L, Phillips RP, Novick KA. 2016 High atmospheric demand for water can limit forest carbon uptake and transpiration as severely as dry soil. *Geophys. Res. Lett.* **43**, 9686–9695. (doi:10.1002/2016GL069416)
40. Reichstein M *et al.* 2002 Severe drought effects on ecosystem CO_2 and H_2O fluxes at three Mediterranean evergreen sites: revision of current hypotheses? *Glob. Change Biol.* **8**, 999–1017. (doi:10.1046/j.1365-2486.2002.00530.x)
41. Fontes CG *et al.* 2018 Dry and hot: the hydraulic consequences of a climate change–type drought for Amazonian trees. *Phil. Trans. R. Soc. B* **373**, 20180209. (doi:10.1098/rstb.2018.0209)
42. Besson CK *et al.* 2014 Cork oak physiological responses to manipulated water availability in a Mediterranean woodland. *Agric. For. Meteorol.* **184**, 230–242. (doi:10.1016/j.agrformet.2013.10.004)
43. Grossiord C *et al.* 2017 Precipitation, not air temperature, drives functional responses of trees in semi-arid ecosystems. *J. Ecol.* **105**, 163–175. (doi:10.1111/1365-2745.12662)